Effect of Volatile Boron Species on the Electrocatalytic Activity of Cathodes of Solid Oxide Fuel Cells: III. $Ba_{0.5}Sr_{0.5}Co_{0.8}Fe_{0.2}O_{3-\delta}$ Electrodes

Kongfa Chen,[a] Junji Hyodo,[b] Kane M. O'Donnell,[c] William Rickard,[c] Tatsumi Ishihara,[b,d] San Ping Jiang [a,*]

[a] Fuels and Energy Technology Institute & Department of Chemical Engineering, Curtin University, Perth, WA 6102, Australia

[b] Department of Applied Chemistry, Faculty of Engineering, Kyushu University, Motooka 744, Nishi-ku, Fukuoka, 819-0395, Japan

[c] Department of Imaging and Applied Physics, Curtin University, Perth, WA 6102, Australia

[d] International Institute for Carbon-Neutral Energy Research (WPI-I2CNER), Kyushu University, Motooka 744, Nishi-ku, Fukuoka, 819-0395, Japan

Abstract

The effect of volatile boron species on the electrocatalytic activity, microstructure and phase stability of $Ba_{0.5}Sr_{0.5}Co_{0.8}Fe_{0.2}O_{3-\delta}$ (BSCF) cathodes has been studied. The cathodes were heat-treated at 800°C for 7 days in air in the presence of boron species vaporized from borosilicate glass, and were characterized by EIS, SEM, AFM, SIMS, XRD, XPS and ICP-OES. The results have shown that after the heat-treatment in the presence of borosilicate glass, boron deposition occurs mainly on the region near electrode surface, leading to the significant Ba and in particular Sr segregation, microstructure change and phase decomposition. On the other hand, the microstructure of the inner electrode layer is almost intact. Electrode polarization resistance, R_E, of an as-prepared BSCF cathode is 0.93 and 0.23 Ω cm^2 at 650 and 800 °C, respectively, and changes to 2.08 and 0.15 Ω cm^2 after

* Corresponding author. Tel.: +61 8 9266 9804; fax: +61 8 9266 1138.
Email address: s.jiang@curtin.edu.au (S.P. Jiang).

heat-treatment at 800 ^{o}C for 7 days in the presence of borosilicate glass, respectively. The increase in R_E for the O_2 reduction reaction on BSCF is much lower than that observed on $La_{0.6}Sr_{0.4}Co_{0.2}Fe_{0.8}O_{3-\delta}$ (LSCF) cathodes, indicating that BSCF cathodes have a much better tolerance towards boron deposition and poisoning. The limited attack of volatile boron species on BSCF is most likely related to the much slower kinetics of the formation of strontium and barium borates as compared to the formation of lanthanum borates. This study provides a significant insight into design and development of better contaminant-tolerant cathode materials for durable solid oxide fuel cell (SOFC) technologies.

Keywords: Solid oxide fuel cells; BSCF cathodes; Boron deposition and poisoning; Strontium and barium borates.

1. Introduction

Glass and glass-ceramic-based sealants have been extensively used to seal the edges of planar solid oxide fuel cell (SOFC) stacks with satisfactory gas impermeability over several or several tens of thousands of hours.[1-5] However, boron species from the borosilicate-based glass sealants are volatile under the SOFC operating conditions,[6, 7] and have a significant detrimental effect on the electrocatalytic activity and structural stability of SOFC electrodes.[8-11] We did a series study on boron deposition and poisoning of SOFC cathodes and showed that the presence of volatile boron species causes a significant microstructure damage and electrochemical degradation of $La_{0.8}Sr_{0.2}MnO_3$ (LSM) and $La_{0.6}Sr_{0.4}Co_{0.2}Fe_{0.8}O_{3-\delta}$ (LSCF) cathodes.[12, 13] Boron preferentially reacts with the A-site cations in particular lanthanum to form lanthanum borates, $LaBO_3$, leading to the collapse of the perovskite structure. In the case of LSM cathodes, the reaction between boron and LSM occurs primarily on the surface and the rate of the $LaBO_3$ formation reaction is very low.[12]

On the other hand, boron has a substantially higher reactivity with the LSCF cathodes and the interaction results in the disintegration and decomposition of LSCF perovskite structure, forming $LaBO_3$ and Fe_2O_3.[13] The presence of volatile boron species also results in dramatic surface segregation of La/Sr in the form of borates on LSM and LSCF bar samples.[14] Chemical compatibility results have revealed that boron has a higher reactivity with La_2O_3 as compared to SrO.[15] It is thus anticipated that eliminating lanthanum in the A-site would enhance the boron tolerance of cathodes.

$Ba_{0.5}Sr_{0.5}Co_{0.8}Fe_{0.2}O_{3-\delta}$ (BSCF) perovskite oxide without the A-site lanthanum would be an ideal candidate for the study of the role of A-site cations in the boron deposition and poisoning. BSCF is an excellent mixed ionic and electronic conductor (MIEC) with a high electrocatalytic activity at low temperatures.[16-19] The excellent electrocatatalytic activity is attributed to its high concentration of mobile oxygen vacancies and high oxygen bulk diffusion coefficient.[20] Unfortunately, BSCF is not structurally stable and is vulnerable to the attack by contaminants. The cubic structure of BSCF tends to collapse during the long-term operation at a temperature below 900^{o}C [21-23] and exposure to CO_2 leads to the formation of $(Ba,Sr)CO_3$ carbonates, deteriorating the electrochemical activity of the BSCF cathodes.[24-26] The presence of volatile Cr species from chromia-forming metallic interconnects also deteriorates the electrode microstructure and electrocatalytic activity.[27, 28] In the case of BSCF hollow fibers for oxygen separation, the use of sulfur-containing polymer in the BSCF slurry can result in formation of barium sulfate in the fibers.[29] However, there have been so far no literature reports regarding the impact of volatile boron species on the electrocatalytic activity and structural stability of BSCF electrodes. In the third part of this series, the electrocatalytic activity, microstructure and phase stability of BSCF cathodes were studied in detail in the presence of volatile boron species. The results show that BSCF cathodes are not chemically compatible with the boron species, but show a relatively higher tolerance towards boron as

compared to that of LSCF cathodes.

2. Experimental

$Gd_{0.1}Ce_{0.9}O_{1.95}$ (GDC) electrolytes were prepared from GDC powder (AGC Seimi Chemical Co. Ltd, Japan). GDC powder was compacted into pellets and sintered at 1450°C for 5 h. The sintered pellets were 1.0 mm in thickness and 19 mm in diameter. $Ba_{0.5}Sr_{0.5}Co_{0.8}Fe_{0.2}O_{3-\delta}$ (BSCF) cathodes were prepared by combined citrate and EDTA complexing method. The starting chemicals were $Ba(NO_3)_2$ (99%, Alfa-Aesar), $Sr(NO_3)_2$ (99%, Sigma-Aldrich), $Co(NO_3)_2 \cdot 6H_2O$ (98.0-102.0%, Alfa-Aesar), $Fe(NO_3)_3 \cdot 9H_2O$ (98%, Chem Supply), citric acid (99.5%, Chem Supply), EDTA (99%, Acros Organics), and ammonia (28%, Ajax Finechem). The molar ratio of metal ions/citric acid/EDTA was 1:1.5:1. The resultant powder was calcined at 950°C in air for 4 h, and the formation of the desired cubic perovskite phase was confirmed by X-ray diffractometry (XRD, Bruker D8 Advance). The as-prepared BSCF powder was mixed with ink vehicle (Fuel Cell Materials, USA) in a weight ratio of 1:1 to form a BSCF ink. The ink was applied on the GDC pellets by slurry coating, and sintered at 1000ºC in air for 2 h. The thickness of the BSCF coating was 10-20 μm and the electrode area was 0.5 cm^2. To facilitate the observation of microstructure changes and surface chemistry characterizations, BSCF bar samples were also prepared. BSCF powder was compacted at a pressure of 110 MPa to form rectangular bars and sintered at 1100ºC in air for 5 h. The dimensions of the sintered BSCF bar samples were 21.4 mm × 6.7 mm × 0.64 mm.

BSCF cathodes and bar samples were placed in a quartz tube furnace, and heat-treated at 800°C under static environmental air for 7 days in the presence of volatile boron species. A borosilicate glass, Spheriglass 3000E (52.5% SiO_2, 8.6% B_2O_3, 14.5% Al_2O_3, 22.5% CaO, 1.2% MgO, 0.3% Na_2O, 0.2% K_2O, and 0.2% Fe/Fe_2O_3, Potters Industries LLC, USA) was used as the source of boron. BSCF cathodes and glass powder were placed side by side in

separated alumina boats. For comparison, the BSCF samples were also heat-treated in the absence of borosilicate glass powder under identical conditions. The experimental setup can be found elsewhere.[12]

The electrochemical activities of BSCF cathodes were conducted with a three-electrode method using a Gamry Reference 3000 Potentiostat. Pt mesh was placed on the BSCF cathodes as the current collector. Impedance curves were recorded under open circuit with frequency range from 0.1 Hz to 100 kHz and the signal amplitude of 10 mV. Electrode polarization resistance, R_E was measured by the differences between the high and low frequency intercepts, and electrode ohmic resistance, R_Ω was obtained from the high frequency intercept. To ensure the reproducibility, 2-3 samples were tested.

Microstructure and element analysis of the samples were examined using scanning electron microscopy (SEM, Zeiss Neon 40EsB) equipped with a backscattered electron detector (BSD) as well as an energy dispersive X-ray analysis (EDS) system. Topography of bar samples was examined by intermittent contact mode atomic force microscopy (AFM: alpha 300 SAR, WITec GmbH, Ulm Germany; probe: silicon probe, spring constant 40 N/m). Line-scan and depth profiles of bar samples were probed by secondary ion mass spectroscopy (SIMS, ATOMIKA-4100). The phase was characterized by XRD. X-ray photoelectron spectroscopy (XPS) was carried out using a Kratos AXIS Ultra DLD system, with monochromated Al Kα X-rays (photon energy 1486.7 eV), a 110 μm aperture and a pass energy of 20 eV. The XPS spectra were calibrated by C 1s peak at 284.8 eV. BSCF cathodes were dissolved by a 3 M HCl solution and the composition was analyzed using inductively coupled plasma optical emission spectrometry (ICP-OES, Optima DV 7300 ICP-OES, PerkinElmer).

To study the chemical compatibility between barium/strontium oxide and boron oxide, oxide couples of BaO, SrO and BaO-SrO mixture (1:1, mol/mol) with 30 wt% B_2O_3 were

mixed, using $BaCO_3$ (≥99%, Sigma-Aldrich), SrO (obtained by decomposing $Sr(NO_3)_2$ at 800°C for 2 h, 99%, Sigma-Aldrich), and H_3BO_3 (≥99.5%, Sigma-Aldrich) as the starting material. The oxide couples were heat-treated at 800°C in air for 20 h and the phase of the oxide couples was analyzed by XRD.

3. Results and Discussion

3.1. Electrochemical performance of BSCF cathodes

Figure 1 shows the impedance responses for the O_2 reduction reaction on BSCF cathodes before and after heat-treated at 800°C for 7 days. R_E of as-prepared BSCF cathode is 0.93 Ω cm^2 at 650°C (Fig. 1a), and is 0.79 Ω cm^2 after heat-treated in the absence of borosilicate glass for 7 days (Fig. 1b). After the heat-treatment in the presence of borosilicate glass, R_E reaches 2.08 Ω cm^2 (Fig. 1c), higher than 0.79 Ω cm^2 of the cathode heat-treated in the absence of borosilicate glass. On the other hand, at a higher test temperature of 800°C, R_E of the cathode after heat-treated in the presence of borosilicate glass is 0.15 Ω cm^2 (Fig. 1f), close to 0.13 Ω cm^2 of the cathode heat-treated in the absence of borosilicate glass (Fig. 1e). Both the R_E values are smaller than 0.23 Ω cm^2 of the as-prepared cathode (Fig. 1d). This indicates that the effect of boron contamination on the BSCF electrode activity is dependent on the operating temperature. Nevertheless, heat-treatment in the presence of borosilicate glass results in an increase of R_Ω regardless of the test temperature. For the BSCF cathode after the heat-treatment in the absence of borosilicate glass for 7 days, R_Ω is ~3.3 Ω cm^2 at 650 °C and ~1.75 Ω cm^2 at 800 °C, similar to that measured on the as-prepared BSCF cathode. After the heat-treatment in the presence of borosilicate glass for 7 days, R_Ω increases significantly to 7.5 Ω cm^2 at 650 °C and 2.8 Ω cm^2 at 800°C. This indicates the electrode electrical conductivity of the BSCF cathodes is significantly degraded in the presence of borosilicate glass. However, the increase in the R_E and R_Ω for the reaction on the BSCF

cathodes is substantially smaller than that observed on LSCF cathodes under identical conditions. For example, for the LSCF cathodes after the heat-treatment in the presence of borosilicate glass at 800 ^{o}C for 7 days, R_E and R_Ω is 84 Ω cm^2 and 73 Ω cm^2, respectively[13], substantially higher than 0.15 Ω cm^2 and 2.8 Ω cm^2 measured on the BSCF cathodes under identical heat-treatment and test conditions.

Figure 2 shows the activation energy plots of the BSCF cathodes. The activation energy (E_a) obtained from the slopes of the curves is 82 ± 3 kJ mol^{-1} for the O_2 reduction reaction on as-prepared BSCF cathode. This is close to the E_a of 81.8-108 kJ mol^{-1} reported in the literature.[30-32] E_a increases to 102 ± 9 and 126 ± 11 kJ mol^{-1} after the heat-treatment in the absence and presence of borosilicate glass, respectively. This indicates that the heat-treatment particularly in the presence of borosilicate glass results in an increase of activation energy for the O_2 reduction reaction on BSCF cathodes.

3.2. Microstructure

Figure 3 shows the SEM micrographs of BSCF cathodes before and after heat-treatment in the absence and presence of borosilicate glass powders at 800 ^{o}C for 7 days. The microstructure of an as-prepared BSCF cathode is characterized by interconnected spherical particles in a size range of 2.2-5.8 μm, and there are crystal facets on the particle surface (Fig. 3a and b). Formation of plate-like particles is observed at the grain boundaries (indicated by arrows, Fig. 3a), and the BSCF particle surface is discretely covered by nanoparticles in the size range of 100-200 nm (Fig. 3a and b). After heat-treatment at 800^{o}C for 7 days in the absence of borosilicate glass (Fig. 3c and d), the shape of BSCF particles is no longer spherical and the particle surface appears smooth with much less nanoparticles as compared to the as-prepared electrode. Irregularly shaped particles in the size range of 0.4-2 μm are also observed on the surface and grain boundaries of BSCF particles (indicated by arrows,

Fig. 3c and d). This indicates the rearrangement of BSCF surface structure during the heat-treatment at 800^{o}C in air. In the case of heat-treatment in the presence of borosilicate glass for 7 days, the BSCF particles on the electrode surface are broken into smaller grains in the size range of 0.3-2 μm (Fig. 3e). However, such a dramatic microstructure change appears to be much less pronounced at the electrode/electrolyte interface region (Fig. 3f). There are formations of clear crystal facets on the BSCF particles but particles are intact, very different from that observed on the electrode surface. This indicates that the reaction between the boron species and BSCF starts at the exposed outmost layer and may slowly and progressively propagate into the bulk of the BSCF cathode.

The depth of the boron reaction layer of the BSCF cathodes after the heat-treatment at 800^{o}C for 7 days in the presence of borosilicate glass was further analyzed by SEM and SIMS (see Fig.4). The microstructure of the cross-section of BSCF cathode is characterized by two distinct regions. The outer layer (region I) with a thickness of ~11 μm experiences significant microstructure changes, while the inner layer adjacent to the electrolyte, region II with a thickness of ~12 μm, experiences a much less microstructure change. The SIMS line scan of the cross-section of the cathode shows that boron species is primarily deposited on the region I, while very little boron is in the inner layer, i.e., the region II. The prominent boron presence in the region I explains the occurrence of more severe microstructure change in the outer electrode surface region (Fig. 3e), as compared to that at the electrode/electrolyte interface region (Fig. 3f). The boron content in the BSCF cathodes after the heat-treatment at 800^{o}C for 7 days in the presence of borosilicate glass was 1.04 ± 0.07 wt%, based on the ICP-OES analysis, while no boron was detectable in the as-prepared BSCF cathodes and the cathodes after heat-treated in the absence of borosilicate glass at 800^{o}C for 7 days. The clear and distinct regions I and II with significant differences in microstructural change and boron concentration indicates that boron deposition and poisoning is staged and may be limited to

the regions close to the surface.

The effect of volatile boron species on the microstructure and composition was also studied on the dense BSCF bar samples. Figure 5 shows the AFM micrographs of BSCF bar samples before and after the heat-treatment in the absence and presence of borosilicate glass at 800 ^{o}C for 7 days. The as-prepared BSCF bar sample was well sintered with large grains in the size range of 11-52 μm (Fig.5a). The BSCF grains have distinct crystal facets and are covered by fine nanoparticles in the range of 250-400 nm (Fig. 5b). After the heat-treatment in the absence of borosilicate glass for 7 days, the BSCF grains become somewhat cleaner with substantially reduced number of nanoparticles on the surface (Fig. 5c and d). Formation of plate-like particles is observed along the grain boundaries. On the other hand, after the heat-treatment in the presence of borosilicate glass at 800 ^{o}C for 7 days, the original large BSCF grains were broken into small grains in the size range of 0.3-4.2 μm (Fig. 5e and f). The microstructure change of BSCF bar samples is similar to that observed on the porous BSCF electrodes (Fig. 3).

Figure 6 shows the SEM and BSD micrographs of the cross section of a BSCF bar sample and corresponding EDS analysis after heat-treatment at 800 ^{o}C for 7 days in the presence of borosilicate glass. The microstructure of the cross section of the BSCF sample can be clearly separated into three regions. The outmost layer (region I, ~5 μm thick) is dense, however, the middle layer (region II, ~9 μm thick) is porous and consists of small and plate-like particles (Fig. 6a). The inner layer (region III) is dense and smooth with large particle size, which represents the typical morphology of as-prepared BSCF bar sample (see Fig. 5a). The BSD micrograph again indicates the existence of three regions (Fig. 6b). Region I is a little darker than the other two regions, indicating a reduction of the average atomic number of this region. In the case of LSM and LSCF bar samples after the heat-treatment at 800 ^{o}C for 7 days in the presence of borosilicate glass, BSD micrograph shows a much darker outmost layer as

compared to the inner layer due to the significant formation of lanthanum borates [14]. The SIMS depth profiles below also show the significant deposition of boron in the outmost layer, but the relatively light darkness indicates that the amount of deposited boron is much less than that observed in the case of LSM and LSCF materials.

EDS analysis was conducted on the three regions of the BSCF bar sample (Fig. 6c). Position 3 in the Region III shows a typical spectrum of as-prepared BSCF composition. The ratios of peak intensities of $Sr_{L\alpha}/Ba_{L\alpha}$, $Sr_{L\alpha}/(Co_{K\alpha1}+Fe_{K\alpha2})$ and $Ba_{L\alpha}/(Co_{K\alpha1}+Fe_{K\alpha2})$ is 1.34, 1.70 and 1.27, respectively. In the case of position 2 in the region II, the ratios of $Sr_{L\alpha}/Ba_{L\alpha}$, $Sr_{L\alpha}/(Co_{K\alpha1}+Fe_{K\alpha2})$ and $Ba_{L\alpha}/(Co_{K\alpha1}+Fe_{K\alpha2})$ is 0.85, 0.85 and 0.99, respectively, lower than those in region III. This indicates the loss of Ba and in particular Sr in region II. On the contrary, position 1 in the region I has predominantly high intensity Ba and Sr peaks, but with negligible Co and Fe peaks. The $Sr_{L\alpha}/Ba_{L\alpha}$ ratio in region I is 2.29, much higher than 0.85 and 1.34 probed in regions II and III, respectively. This indicates the significant segregation of Ba and in particular Sr from region II to region I. The substantial loss of Ba and in particular Sr in region II may be the reason for the formation of porous inner layer most likely due to the disintegration of the BSCF microstructure.

Figure 7 shows the SIMS depth profiles starting from the surface of BSCF bar samples. For the as-prepared BSCF bar sample, the cation distributions of BSCF are more or less stable regardless of the probing depth, and no boron species is detected (Fig. 7a). The same can also be said for the BSCF bar sample after the heat-treatment at 800^{o}C for 7 days in the absence of borosilicate glass (Fig. 7b). On the other hand, after the heat-treatment at 800^{o}C for 7 days in the presence of borosilicate glass, boron distributes mainly in the near surface region of BSCF bar sample within a reaction depth of ~0.75 μm. Moreover, Sr also has a very high intensity in the near surface region, similar to the concentration profile of boron, whereas the intensities of Ba and in particular Co and Fe are significantly reduced. This

indicates the surface segregation of Ba and in particular Sr, in an agreement with the EDS results (Fig. 6c).

3.3. Phase stability

Figure 8 shows the XRD patterns of BSCF cathodes before and after the heat-treatment at 800^{o}C for 7 days. XRD analysis was conducted on the intact electrodes (i.e. they were not powderised) and as such the data is representative of the average composition of the top few microns of the samples. In the case of an as-prepared BSCF cathode, there are typical diffraction peaks of perovskite BSCF from the electrode and cubic GDC from the electrolyte substrate (Fig. 8a). After the heat-treatment at 800^{o}C for 7 days in the absence of borosilicate glass, additional peaks associated with a hexagonal perovskite $Ba_{0.5}Sr_{0.5}CoO_3$ appear (Fig. 8b). The formation of $Ba_{0.5}Sr_{0.5}CoO_3$ indicates that BSCF phase is not stable at 800 ^{o}C, consistent with the reported phase instability of BSCF at operating temperature below 900^{o}C.[21, 33, 34] The phase instability explains the significant microstructure changes of BSCF after the heat-treatment at 800 ^{o}C in the absence of borosilicate glass for 7 days (Fig. 3c and Fig. 5c). On the other hand, in the case of heat-treatment for 7 days in the presence of borosilicate glass, the BSCF diffraction peaks disappear completely, and there are formations of many new small peaks (Fig. 8c). The new peaks are originated from a number of compounds such as $BaFeO_{2.25}$, $BaFeO_{2.64}$, $BaFeO_3$, $BaCO_3$, $Ba_3Co_2Fe_{24}O_{41}$ and $Sr_3FeO_{6.69}$. This indicates that the heat-treatment in the presence of volatile boron species from the borosilicate glass leads to the disintegration and decomposition of BSCF perovskite structure. It is worthwhile to note that no distinctive borate phases have been detected after the heat-treatment in the presence of borosilicate glass, though boron deposition has been confirmed by ICP-OES and SIMS (Fig. 7). This indicates that the boron is present in poorly ordered / amorphous phases or is interstitial in the other phases.

Figure 9 shows the XRD patterns of the oxide couples of $BaO\text{-}H_3BO_3$, $SrO\text{-}H_3BO_3$ and $BaO\text{-}SrO\text{-}H_3BO_3$ after the heat-treatment at 800°C in air for 20 h. In the case of $BaO\text{-}H_3BO_3$ oxide couple, BaB_2O_4 is the main reaction product (curve a, Fig.9); while the reaction product of the $SrO\text{-}H_3BO_3$ oxide couple consists of SrB_2O_4 and $Sr_2B_2O_5$ (curve b, Fig.9). In the case of $BaO\text{-}SrO\text{-}H_3BO_3$ oxide couple, $(Sr_{1.16}Ba_{1.84})(B_3O_6)_2$ and SrB_2O_4 are formed after the heat-treatment (curve c, Fig.9). The XRD results indicate that boron oxide is very reactive with BaO and SrO, forming barium and strontium borates at 800°C.

Figure 10 shows the XPS spectra attained from the surface of BSCF cathodes before and after the heat-treatment at 800°C for 7 days, and the quantitative results are listed in Table 1. XPS did not detect the deposition or poisoning of Si species, consistent with EDS and SIMS profile analysis. This indicates that under the conditions of the present study, the moist content in the environmental air would be very low, and thus the deposition and poisoning of LSCF cathodes by gaseous $Si(OH)_4$ as observed by Bucher et al [35, 36] under high steam concentrations is not an issue in this case. The as-prepared BSCF cathode and the cathode after the heat-treatment in the absence of borosilicate glass show no boron peaks, and there are observations of only $Ba4p_{1/2}$ peaks in the binding energy range of 185-200 eV. For the BSCF cathode after the heat-treatment at 800 °C in the presence of borosilicate glass for 7 days, a B1s peak at 190.2 eV appears which overlaps with the $Ba4p_{1/2}$ peaks. The superimposition of B1s and $Ba4p_{1/2}$ peaks has also been reported.[37] The B1s peak at 190.2 eV is most likely originates from borates.[38] The binding energy for Ba4p, Sr3d and O1s does not change significantly for the BSCF cathodes after the heat-treatment in the absence of borosilicate glass, though the relative peak intensities are different. The variations of Ba4p and Sr3d peaks of the BSCF after the heat-treatment at 800 °C in the absence of borosilicate glass are most likely attributed to the formation of $Ba_{0.5}Sr_{0.5}CoO_3$ phase (Fig. 8b), and surface segregation of Ba and Sr after the heat-treatment (Table 1). After the heat-treatment at 800 °C

in the presence of borosilicate glass, the Ba4p, Sr3d and O1s peaks are widened and the peaks' shape also varied significantly, most likely due to the formation of borates. After exposure to the volatile boron species, the amounts of Ba and Sr increase on the BSCF particles' surface (Table 1), which is consistent with the EDS results (Fig. 6c).

3.4. Mechanism of boron deposition and poisoning

The present study has shown that the deposition of volatile boron species leads to significant Ba and in particular Sr segregation on the surface of BSCF electrodes. Sr and Ba surface segregation under the present heat-treatment conditions has been demonstrated by the quantitative XPS (Table 1), EDS and SIMS results, in agreement with the literature report.[39] Oxide couple study has shown that Sr and Ba oxides are not chemically compatible with boron, forming Sr and Ba borates (Fig. 9). On the other hand, the volatile boron species tends to react with the segregated Sr and Ba, forming B/Sr-containing amorphous phases and $Ba(Co,Fe)O_x$ or $BaFeO_x$. This in turn accelerates the segregation of Sr and Ba to the surface, as indicated by the disintegration of the BSCF and formation of porous inner layer (i.e., region II) of BSCF bar samples after the heat-treatment at 800 ^oC in the presence of borosilicate glass (Fig. 6). The excess depletion of A-site cations will cause substantial nonstiochiometry and thereby decomposition of the BSCF pervoskite structure. The detection of Sr/Ba borates in the case of solid oxide couples (Fig.9) and not in the BSCF/gaseous boron species system (Fig.8) indicates that the phase contact between the reactive species plays an important role in the formation of Sr/Ba borates. The presence of the gaseous boron species is less favorable for the formation of Sr/Ba borates as compared to the solid boron oxides. The reaction between BSCF and volatile boron species such as BO_2 in dry air can be expressed by following equation:

$$BO_{2,\,gas} + Ba_{0.5}Sr_{0.5}Co_{0.8}Fe_{0.2}O_{3-\delta} \rightarrow \text{B/Sr-containing amorphous compounds} + BaFeO_x +$$

$$Ba(Fe,Co)O_x \qquad (1)$$

On the other hand, the BSCF cathode is much more tolerant towards boron as compared to the LSCF cathodes. After heat-treated at 800^{o}C for 7 days in the presence of borosilicate glass, the amount of boron deposition in BSCF electrode is 1.04 ± 0.07 wt%, much lower than 3.5 wt% in the case of LSCF electrode.[13] Compared to the significant lanthanum borate formation in the case of LSCF electrode, no detectable barium borate X-ray diffraction peaks are observed in the BSCF electrode. Despite the fact that the BSCF cathode undergoes dramatic microstructure changes and phase decomposition on the outmost layer, the outmost layer appears to act as a buffer/trapping layer to protect the inner electrode region from the attack by boron. The relative intact electrode/electrolyte interface region (region II as shown in Fig. 4) could still function as an electrochemically active region. This is supported by the much lower variation of the R_E and R_Ω values for the O_2 reduction reaction on BSCF cathodes, as compared to their substantial increase for the reaction on LSCF under identical the heat-treatment conditions.[13]

Previous studies have shown that partial replacement of Sr by Ba in the LSCF perovskite structure leads to a significantly reduced chromium poisoning effect on the electrode activity and stability, primarily due to the fact that the formation and grain growth of $BaCr_2O_4$ phase between gaseous Cr species and chromia forming nuclei is kinetically a very slow process [40, 41]. Chemical compatibility study also showed that the chemical activity between boron and La_2O_3 is significantly higher than that with SrO.[15] In the case of SrO-La_2O_3-Al_2O_3-B_2O_3-SiO_2 glass, the formation of $LaBO_3$ phase rather than SrB_2O_4 phase is most significant, degrading the thermal stability and contributing to the devitrification of the glass.[42, 43] In a 20%SrO–20%BaO–xB_2O_3–(60%-x)SiO_2 glass, Zhang and Zou reported the formation of strontium borate, SrB_2O_4, rather than barium borate with increasing boron content,[44] indicating the low reactivity between barium and boron for the barium borate formation. Thus,

the fundamental reason for the much less boron deposition and poisoning of BSCF as compared to that on LSCF is the much slower kinetics of the formation of barium and strontium borates as compared to the formation of lanthanum borate.

4. Conclusions

Effect of volatile boron species on the electrochemical activity and microstructure of BSCF cathodes has been studied on both porous and dense BSCF bar samples. The BSCF cathode materials were heat-treated at 800^{o}C for 7 days in the presence of borosilicate glass. Volatile boron species from the borosilicate glass has a significant detrimental effect on the electrocatalytic and structural properties of BSCF materials. Boron deposition will accelerate the Ba and in particular Sr segregation on the BSCF surface, damage the electrode microstructure and decompose the BSCF perovskite structure. However, the boron deposition and poisoning mainly occur on the outmost electrode layer and the relatively intact inner region close to the electrode/electrolyte interface can still function electrochemcially, very different from the almost complete disintegration of the perovskite structure observed on LSCF cathodes under identical experimental conditions. The much lower and limited boron attack on the BSCF cathodes as compared to that on the LSCF is due to the much slower kinetics of Ba/Sr borate formation as compared to the formation of La borates.

Acknowledgements

The project is supported by Curtin University Research Fellowships, Australian Research Council *Linkage Project funding scheme* (project number: LP110200281), Australia. The authors acknowledge the facilities, scientific and technical assistance of the Curtin University Electron Microscope Facility and Curtin X-Ray Laboratory, both of which are partially funded by the University, State and Commonwealth Governments, the WA X-Ray Surface

Analysis Facility, funded by the Australian Research Council LIEF grant (LE120100026), and the Department of Chemistry/Nanochemistry Research Institute, Curtin University.

References:

1. J. Malzbender, P. Batfalsky, R. Vaßen, V. Shemet and F. Tietz, *Journal of Power Sources*, **201**, 196 (2012).
2. J. A. Schuler, Z. Wuillemin, A. Hessler-Wyser, C. Comminges, N. Y. Steiner and J. Van herle, *Journal of Power Sources*, **211**, 177 (2012).
3. N. H. Menzler, F. Han, T. van Gestel, W. Schafbauer, F. Schulze-Kuppers, S. Baumann, S. Uhlenbruck, W. A. Meulenberg, L. Blum and H. P. Buchkremer, *International Journal of Applied Ceramic Technology*, **10**, 421 (2013).
4. F. Smeacetto, M. Salvo, M. Santarelli, P. Leone, G. A. Ortigoza-Villalba, A. Lanzini, L. C. Ajitdoss and M. Ferraris, *International Journal of Hydrogen Energy*, **38**, 588 (2013).
5. Y.-S. Chou, J. W. Stevenson and J.-P. Choi, *Journal of Power Sources*, **255**, 1 (2014).
6. M. J. Snyder, M. G. Mesko and J. E. Shelby, *Journal of Non-Crystalline Solids*, **352**, 669 (2006).
7. T. Zhang, W. G. Fahrenholtz, S. T. Reis and R. K. Brow, *J. Am. Ceram. Soc.*, **91**, 2564 (2008).
8. T. Komatsu, K. Watanabe, M. Arakawa and H. Arai, *Journal of Power Sources*, **193**, 585 (2009).
9. X. D. Zhou, J. W. Templeton, Z. Zhu, Y. S. Chou, G. D. Maupin, Z. Lu, R. K. Brow and J. W. Stevenson, *Journal of the Electrochemical Society*, **157**, B1019 (2010).
10. K. Sasaki, K. Haga, T. Yoshizumi, D. Minematsu, E. Yuki, R. Liu, C. Uryu, T. Oshima, T. Ogura, Y. Shiratori, K. Ito, M. Koyama and K. Yokomoto, *Journal of Power Sources*, **196**, 9130 (2011).
11. K. Chen, N. Ai, C. Lievens, J. Love and S. P. Jiang, *Electrochemistry Communications*, **23**, 129 (2012).
12. K. F. Chen, N. Ai, L. Zhao and S. P. Jiang, *J. Electrochem. Soc.*, **160**, F183 (2013).
13. K. F. Chen, N. Ai, L. Zhao and S. P. Jiang, *J. Electrochem. Soc.*, **160**, F301 (2013).
14. K. Chen, J. Hyodo, L. Zhao, N. Ai, T. Ishihara and S. P. Jiang, *Journal of the Electrochemical Society*, **160**, F1033 (2013).
15. K. Chen, N. Ai and S. P. Jiang, *Fuel Cells*, **13**, 1101 (2013).
16. Z. P. Shao and S. M. Haile, *Nature*, **431**, 170 (2004).
17. W. Zhou, R. Ran and Z. P. Shao, *J. Power Sources*, **192**, 231 (2009).
18. N. Ai, S. P. Jiang, Z. Lu, K. F. Chen and W. H. Su, *J. Electrochem. Soc.*, **157**, B1033 (2010).
19. F. L. Liang, W. Zhou, J. Li and Z. H. Zhu, *Journal of Materials Chemistry A*, **1**, 13746 (2013).
20. S. McIntosh, J. F. Vente, W. G. Haije, D. H. A. Blank and H. J. M. Bouwmeester, *Chem. Mat.*, **18**, 2187 (2006).
21. K. Efimov, Q. Xu and A. Feldhoff, *Chemistry of Materials*, **22**, 5866 (2010).
22. J.-I. Jung and D. D. Edwards, *Journal of the European Ceramic Society*, **32**, 3733 (2012).
23. P. Muller, H. Stormer, M. Meffert, L. Dieterle, C. Niedrig, S. F. Wagner, E. Ivers-Tiffee and D. Gerthsen, *Chemistry of Materials*, **25**, 564 (2013).
24. E. Bucher, A. Egger, G. B. Caraman and W. Sitte, *J. Electrochem. Soc.*, **155**, B1218 (2008).
25. A. Y. Yan, M. Yang, Z. F. Hou, Y. L. Dong and M. J. Cheng, *J. Power Sources*, **185**, 76

(2008).
26. K. Schmale, J. Barthel, M. Bernemann, M. Grunebaum, S. Koops, M. Schmidt, J. Mayer and H. D. Wiemhofer, *Journal of Solid State Electrochemistry*, **17**, 2897 (2013).
27. Y. M. Kim, X. B. Chen, S. P. Jiang and J. Bae, *Electrochemical and Solid State Letters*, **14**, B41 (2011).
28. Y. M. Kim, X. B. Chen, S. P. Jiang and J. Bae, *J. Electrochem. Soc.*, **159**, B185 (2012).
29. A. Leo, S. Smart, S. Liu and J. C. D. da Costa, *Journal of Membrane Science*, **368**, 64 (2011).
30. S. Li, Z. Lü, X. Huang, B. Wei and W. Su, *Journal of Physics and Chemistry of Solids*, **68**, 1707 (2007).
31. D. Chen, C. Huang, R. Ran, H. J. Park, C. Kwak and Z. Shao, *Electrochemistry Communications*, **13**, 197 (2011).
32. L. Wang, R. Merkle and J. Maier, *Journal of The Electrochemical Society*, **157**, B1802 (2010).
33. M. Arnold, T. M. Gesing, J. Martynczuk and A. Feldhoff, *Chemistry of Materials*, **20**, 5851 (2008).
34. Z. Yáng, J. Martynczuk, K. Efimov, A. S. Harvey, A. Infortuna, P. Kocher and L. J. Gauckler, *Chemistry of Materials*, **23**, 3169 (2011).
35. E. Bucher, C. Gspan, F. Hofer and W. Sitte, *Solid State Ionics*, **230**, 7 (2013).
36. E. Bucher, W. Sitte, F. Klauser and E. Bertel, *Solid State Ionics*, **191**, 61 (2011).
37. S. Wersand-Quell, G. Orsal, P. Thévenin and A. Bath, *Thin Solid Films*, **515**, 6507 (2007).
38. M. J. Saly, F. Munnik and C. H. Winter, *Journal of Materials Chemistry*, **20**, 9995 (2010).
39. C. Norman and C. Leach, *J. Membr. Sci.*, **382**, 158 (2011).
40. X. B. Chen, L. Zhang and S. P. Jiang, *Journal of the Electrochemical Society*, **155**, B1093 (2008).
41. Y. Zhen and S. P. Jiang, *J. Power Sources*, **180**, 695 (2008).
42. M. K. Mahapatra, K. Lu and R. J. Bodnar, *Appl. Phys. A*, **95**, 493 (2009).
43. M. K. Mahapatra, K. Lu and W. T. Reynolds Jr, *Journal of Power Sources*, **179**, 106 (2008).
44. T. Zhang and Q. Zou, *Journal of the European Ceramic Society*, **32**, 4009 (2012).

Figure Captions

1. Impedance responses of BSCF cathodes measured at 650^{o}C (left) and 800^{o}C (right) under open circuit: (a,d) as-prepared, (b,e) after the heat-treatment at 800 ^{o}C for 7 days in the absence of borosilicate glass, and (c,f) after the heat-treatment at 800^{o}C for 7 days in the presence of borosilicate glass.
2. Activation energy plots of BSCF cathodes for the O_2 reduction reaction before and after the heat-treatment at 800^{o}C for 7 days in the absence and presence of borosilicate glass.
3. SEM micrographs of surface (left) and BSCF electrode/GDC electrolyte interface region (right) of BSCF cathodes: (a,b) as-prepared, (c,d) after the heat-treatment at 800^{o}C for 7 days in the absence of borosilicate glass, and (e,f) after the heat-treatment at 800^{o}C for 7 days in the presence of borosilicate glass.
4. (a) SEM micrographs of cross section of a BSCF cathode after the heat-treatment at 800^{o}C for 7 days in the presence of borosilicate glass, and (b) the corresponding SIMS line-scan.
5. AFM micrographs of surface of BSCF bar samples: (a,b) as-prepared, (c,d) after the heat-treatment at 800^{o}C for 7 days in the absence of borosilicate glass, and (e,f) after the heat-treatment at 800^{o}C for 7 days in the presence of borosilicate glass. The images on the right are the magnified regions marked on the figures on the left.
6. (a) SEM and (b) BSD micrographs of cross section of a BSCF bar sample after the heat-treatment at 800^{o}C for 7 days in the presence of borosilicate glass, and (c) EDS spectra taken on the positions 1, 2 and 3 of the cross section of the BSCF bar sample as shown in (a).
7. SIMS depth profiles of BSCF bar samples: (a) as-prepared, (b) after the heat-treatment at 800^{o}C for 7 days in the absence of borosilicate glass, and (c) after the heat-treatment at 800^{o}C for 7 days in the presence of borosilicate glass.

8. XRD patterns of BSCF cathodes: (a) as-prepared, (b) after the heat-treatment at 800^{o}C for 7 days in the absence of borosilicate glass, and (c) after the heat-treatment at 800^{o}C for 7 days in the presence of borosilicate glass.
9. XRD patterns of (a) BaO-H_3BO_3, (b) SrO-H_3BO_3, and (c) BaO-SrO-H_3BO_3 oxide couples after sintered at 800^{o}C in air for 20 h.
10. XPS spectra of (A) B1s & Ba4p, (B) Sr 3d and (C) O 1s on surface of BSCF cathodes: (a) as-prepared, (b) after the heat-treatment at 800^{o}C for 7 days in the absence of borosilicate glass, and (c) after the heat-treatment at 800^{o}C for 7 days in the presence of borosilicate glass.

Figure 1.

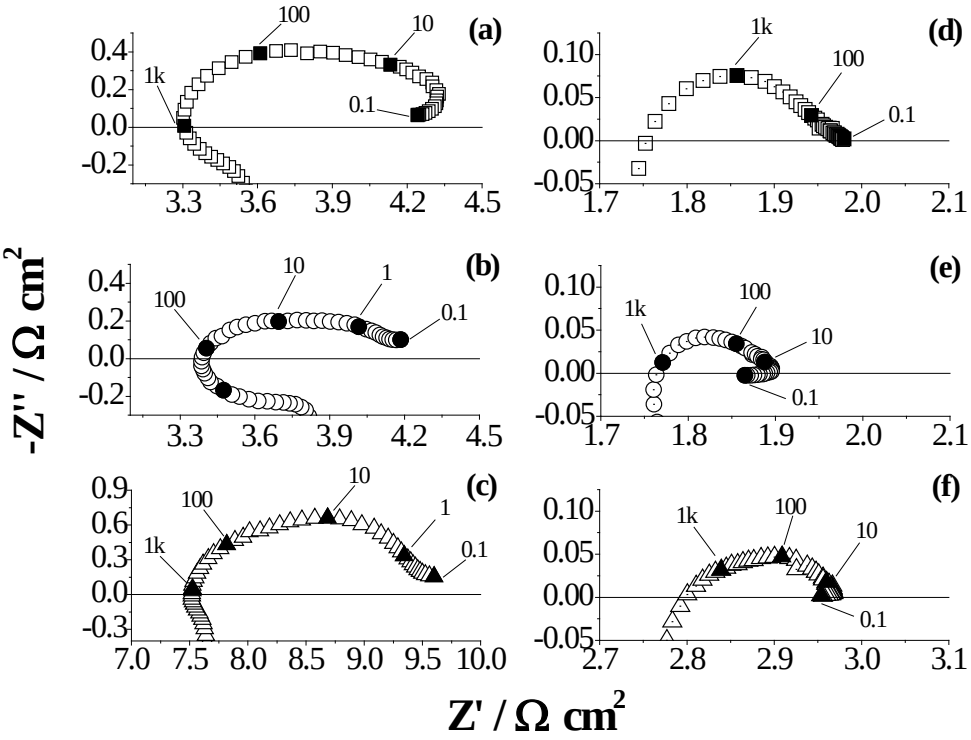

Figure 2.

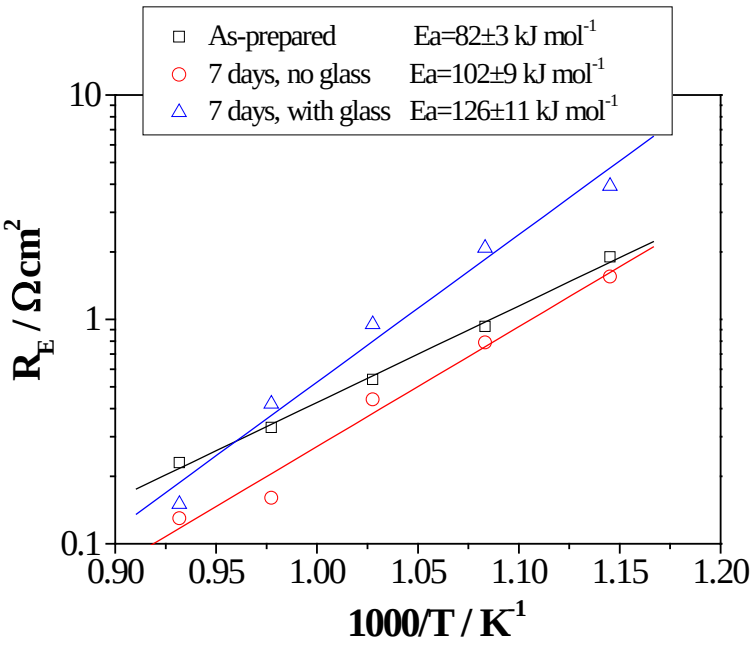
As-prepared Ea=82±3 kJ mol-1
7 days, no glass Ea=102±9 kJ mol-1
7 days, with glass Ea=126±11 kJ mol-1
10
1
0.1
R_E / Ωcm^2
0.90
0.95
1.00
1.05
1.10
1.15
1.20
1000/T / K^-1

Figure 3.

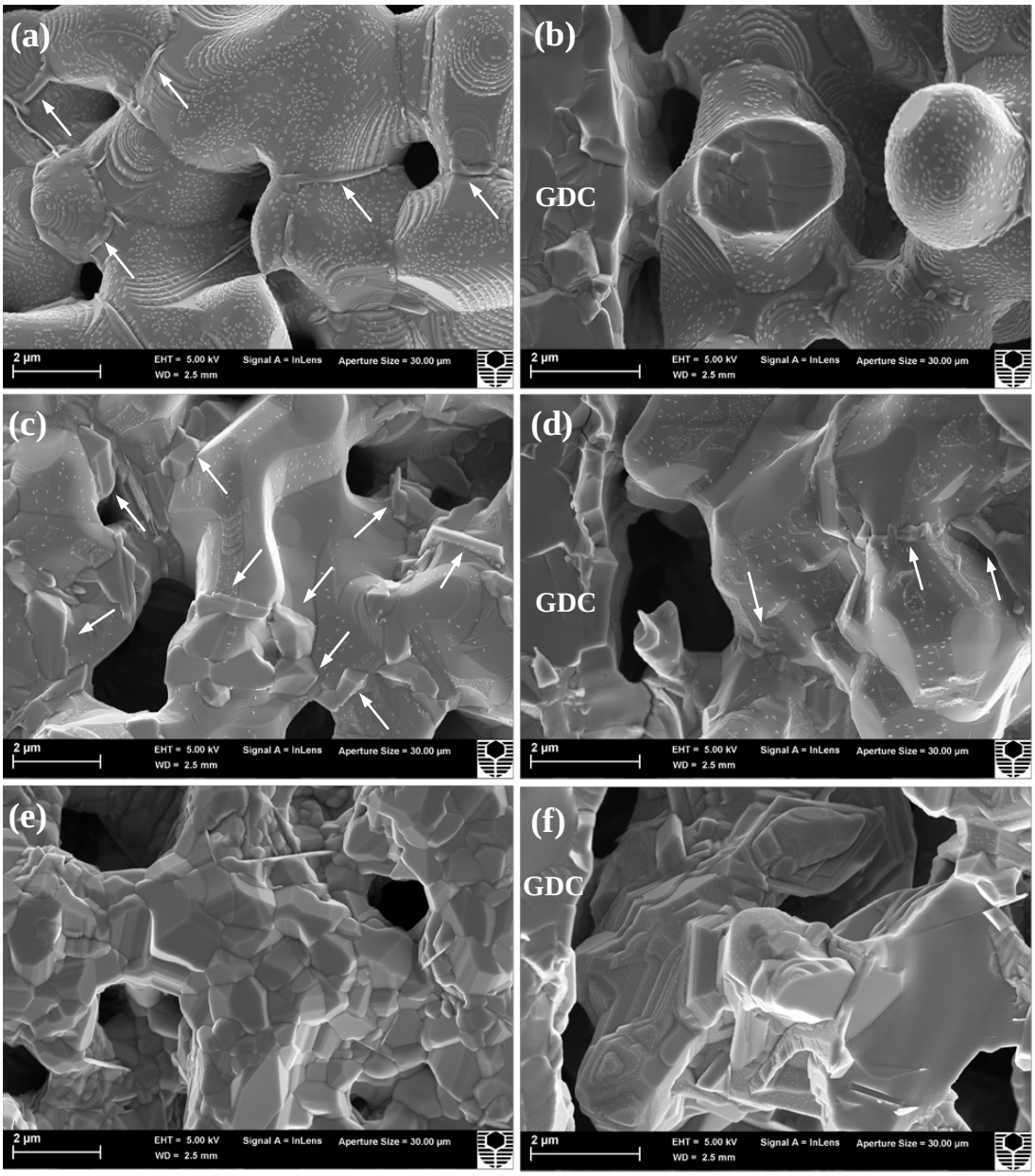
(a)
(b)
GDC
(c)
(d)
GDC
(e)
(f)
GDC
2 µm
EHT = 5.00 kV
WD = 2.5 mm
Signal A = InLens
Aperture Size = 30.00 µm

Figure 4.

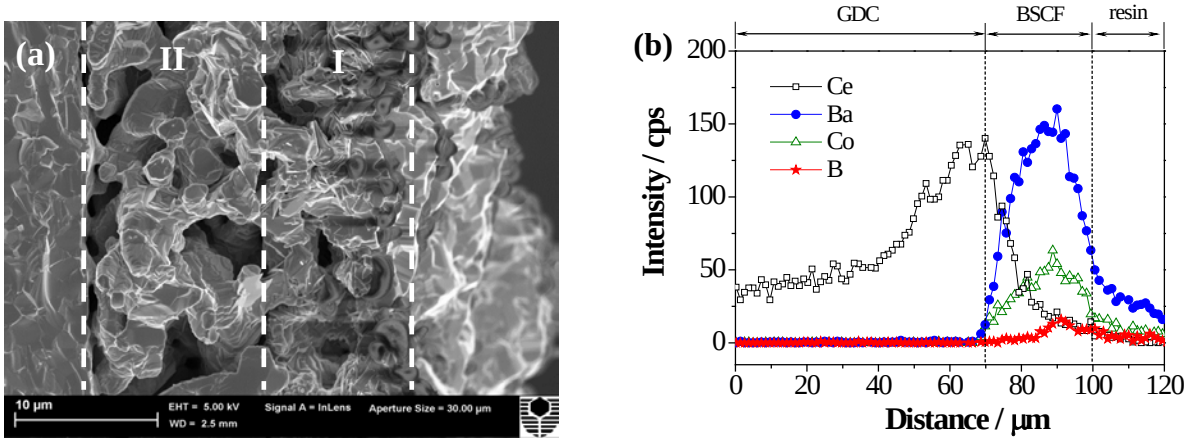
(a)
II
I
10 µm
EHT = 5.00 kV
WD = 2.5 mm
Signal A = InLens
Aperture Size = 30.00 µm
(b)
GDC
BSCF
resin
Ce
Ba
Co
B
Intensity / cps
Distance / µm
0
50
100
150
200
0
20
40
60
80
100
120

Figure 5.

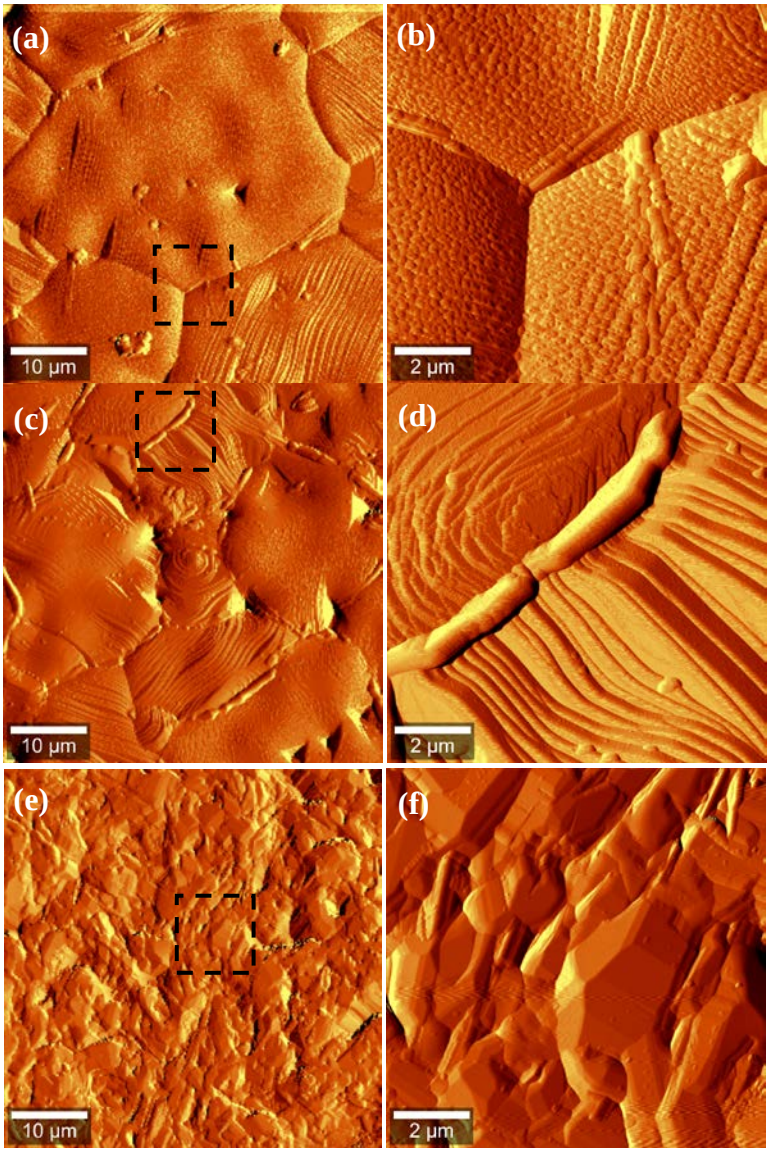

Figure 6.

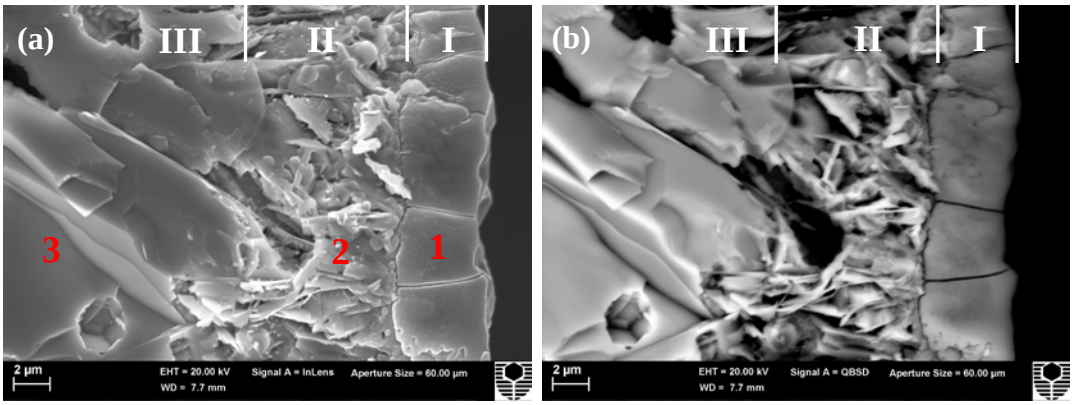
(a)
III
II
I
3
2
1
2 µm
EHT = 20.00 kV
WD = 7.7 mm
Signal A = InLens
Aperture Size = 60.00 µm
(b)
III
II
I
2 µm
EHT = 20.00 kV
WD = 7.7 mm
Signal A = QBSD
Aperture Size = 60.00 µm

(c)

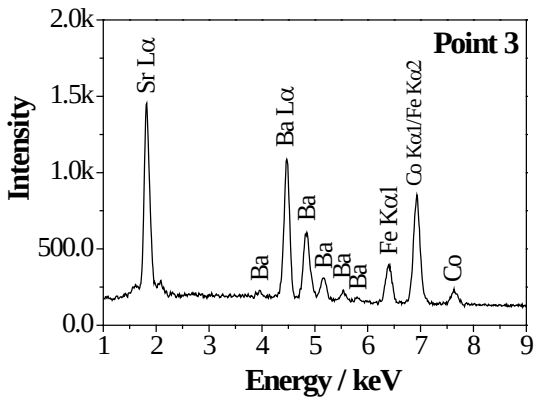
Point 3
Intensity
Energy / keV
Sr Lα
Ba Lα
Ba
Fe Kα1
Co Kα1/Fe Kα2
Co

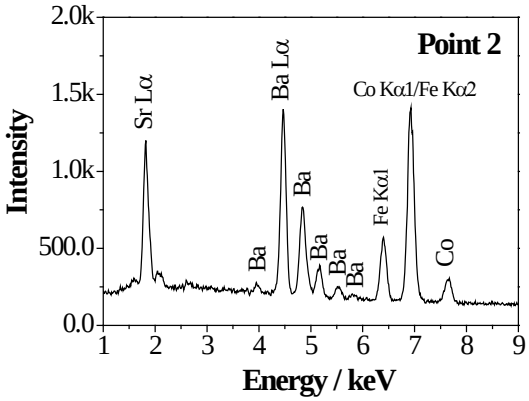
Point 2
Intensity
Energy / keV
Sr Lα
Ba Lα
Ba
Co Kα1/Fe Kα2
Fe Kα1
Co

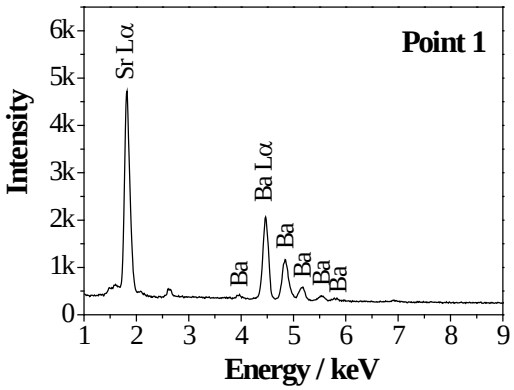
Point 1
Intensity
Energy / keV
Sr Lα
Ba Lα
Ba

Figure 7.

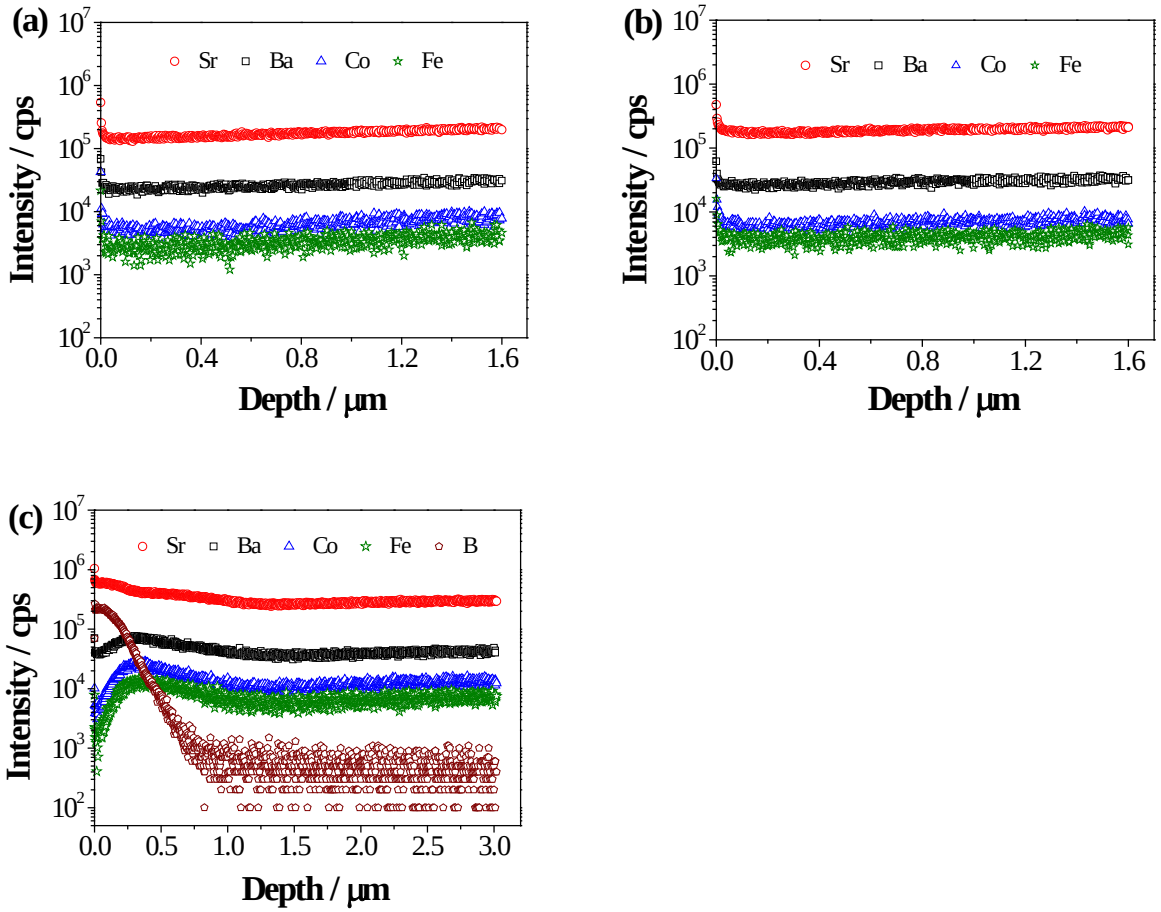

Figure 8.

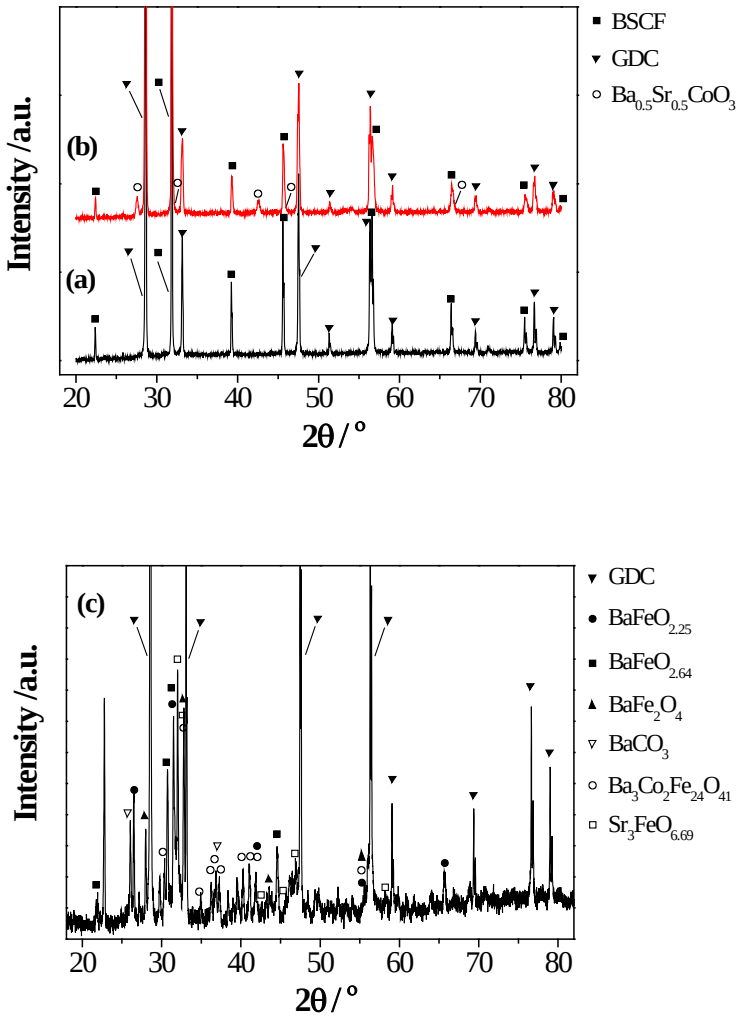
Intensity /a.u.
(b)
(a)
20
30
40
50
60
70
80
2θ / °
BSCF
GDC
Ba0.5Sr0.5CoO3
(c)
Intensity /a.u.
20
30
40
50
60
70
80
2θ / °
GDC
BaFeO2.25
BaFeO2.64
BaFe2O4
BaCO3
Ba3Co2Fe24O41
Sr3FeO6.69

Figure 9.

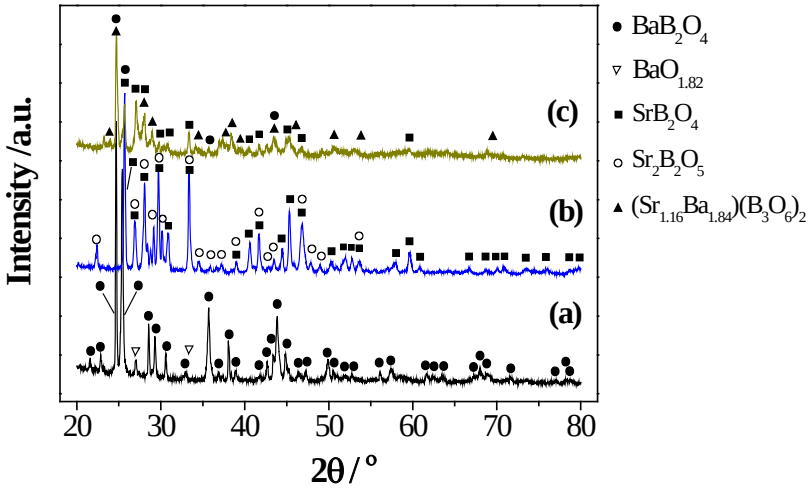
Intensity /a.u.
(c)
(b)
(a)
20
30
40
50
60
70
80
2θ / °
● BaB_2O_4
▿ $BaO_{1.82}$
■ SrB_2O_4
○ $Sr_2B_2O_5$
▲ $(Sr_{1.16}Ba_{1.84})(B_3O_6)_2$

Figure 10.

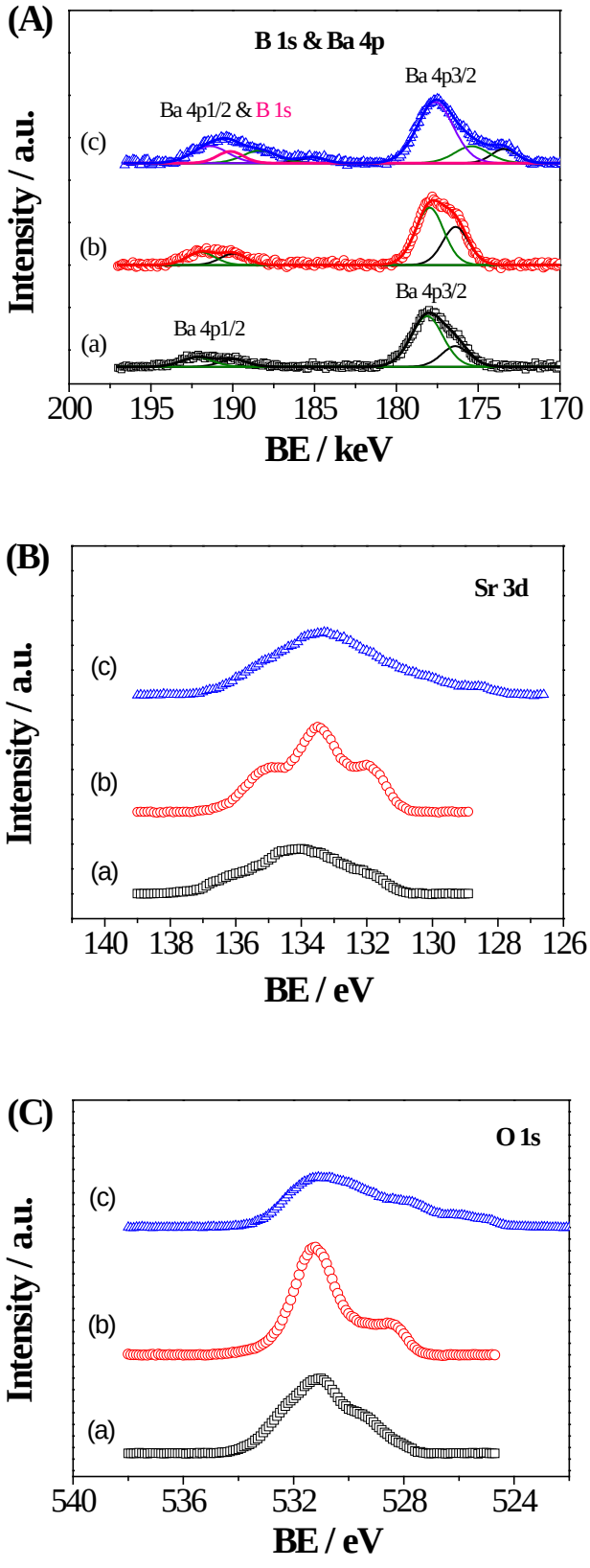
(A)
B 1s & Ba 4p
Ba 4p3/2
Ba 4p1/2 & B 1s
(c)
(b)
Ba 4p3/2
Ba 4p1/2
(a)
Intensity / a.u.
200 195 190 185 180 175 170
BE / keV
(B)
Sr 3d
(c)
(b)
(a)
Intensity / a.u.
140 138 136 134 132 130 128 126
BE / eV
(C)
O 1s
(c)
(b)
(a)
Intensity / a.u.
540 536 532 528 524
BE / eV

Table 1. XPS quantitative analysis of cation distribution on the surface of BSCF cathodes.

Elements	Stoichiometric / mol%	As-prepared / mol%	7 days, without borosilicate glass / mol%	7 days, with borosilicate glass / mol%
Ba	25	23	23	29
Sr	25	30	38	44
Co	40	28	20	20
Fe	10	19	18	7
ICP analysis				
B	0	0	0	1.04 ± 0.07 wt%